ACS Catalysis

Research Article

pubs.acs.org/acscatalysis

Exploring Furfural Catalytic Conversion on Cu(111) from Computation

Yun Shi,[†,‡,§] Yulei Zhu,[†,‡] Yong Yang,[†,‡] Yong-Wang Li,[†,‡] and Haijun Jiao*[,†,∥]

[†]State Key Laboratory of Coal Conversion, Institute of Coal Chemistry, Chinese Academy of Sciences, Taiyuan, 030001, People's Republic of China

[‡]National Energy Center for Coal to Liquids, Synfuels China Co., Ltd, Huairou District, Beijing, 101400, People's Republic of China

[§]University of Chinese Academy of Sciences, No. 19A Yuquan Road, Beijing, 100049, People's Republic of China

[∥]Leibniz-Institut für Katalyse e.V. an der Universität Rostock, Albert-Einstein Strasse 29a, 18059 Rostock, Germany

Supporting Information

ABSTRACT: The full potential energy surface of the catalytic conversion of furfural to 2-methylfuran on the Cu(111) surface has been systematically computed on the basis of density functional theory, including dispersion and zero-point energy corrections. For furfuryl alcohol formation, the more favorable step is the first H addition to the carbon atom of the C═O group, forming an alkoxyl intermediate (F-CHO +H → F-CH_2O); the second H atom addition, leading to furfuryl alcohol formation (F-CH_2O + H → F-CH_2OH), is the rate-determining step. For 2-methylfuran formation from furfuryl alcohol dissociation into surface alkyl (F-CH_2) and OH groups, H_2O formation is the rate-determining step (OH + H → H_2O). Our results explain perfectly the experimentally observed selective formation of furfuryl alcohol and the equilibrium of furfural/furfuryl alcohol conversion under hydrogen-rich conditions as well as the effect of H_2O suppressing furfural conversion. In addition, it is found that dispersion correction (PBE-D3) overestimates the adsorption energies of furfural, furfuryl alcohol, and 2-methylfuran considerably, whereas those of H_2 and H_2O can be reproduced nearly quantitatively. Our results provide insights into Cu-catalyzed furfural selective conversion and broaden our fundamental understanding into deoxygenation reactions of oxygenates involved in the refining of biomass-derived oils.

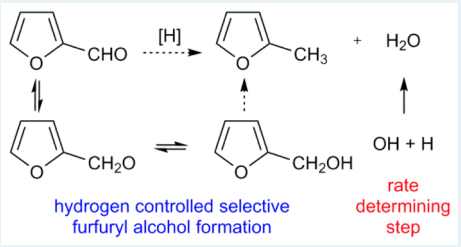

KEYWORDS: *furfural, furfuryl alcohol, 2-methylfuran, DFT, PBE-D3*

1. INTRODUCTION

Owing to the growing energy demand, increasing environmental concerns, and chiefly the declining of petroleum reserves as well as greenhouse gas emissions, new nonfossil resources have attracted considerable and increasing attention. The research with regard to catalytic reactions of unsaturated oxygenates is of great interest because of the prevalence of these compounds as intermediates in the conversion of biomass to fine chemicals and fuels.[1] One class of unsaturated oxygenates, furan derivatives, has received increased attention because of their production from biomass deconstruction.[2,3] Furan derivatives can be used as model compounds for hydrodeoxygenation studies[4] and precursors for liquid alkane fuels,[5−7] resins, and polymers.[8]

Furfural is a simple organic compound that can be derived from a variety of agricultural byproducts, including corncobs, oats, wheat bran, and sawdust. Furfural is usually obtained by acid-catalyzed dehydration of xylose, which is the main building block of hemicellulose, one of the constituents of biomass. Furfural can also be obtained from fast pyrolysis of biomass at moderate temperatures, high heating rates, and short residence times.[9−14] Furfural is one of the numerous oxygenated compounds commonly found in bio-oil.[15−18] Bio-oil has the potential as second-generation biofuel because it can be produced in high volumes without threatening food supplies and biodiversity. Because of its high oxygen and water contents, however, it needs a significant post-treatment before it can be used as fuel.[19,20] It also is necessary to upgrade bio-oil catalytically to improve its storage stability, boiling point range, water solubility and octane number.

As one of the potential routes for bio-oil stabilization, mild hydrogenation eliminates the most reactive oxygenate groups, which in turn are the least desirable components in fuel.[21,22] There are several approaches for furfural conversion. Aldol condensation of furfural with small ketones is a prospective approach to produce larger compounds (C_8−C_{15}) that may fall in fuel ranges.[23−26] High yields of products from direct condensation of furfural with acetone have been obtained in the presence of basic catalysts. Selective hydrogenation of furfural may be an alternative route to increase the stability and to produce compounds as gasoline components. For example, 2-methylfuran is a better additive to gasoline, which could be used as an octane booster (RON = 131).

Since the first effort in catalytic upgrade of furfural,[27] it has been found that the products of furfural chemical transformation

Received: February 12, 2015
Revised: May 15, 2015
Published: May 20, 2015

DOI: 10.1021/acscatal.5b00303
ACS Catal. 2015, 5, 4020−4032

Table 1. Influence of Slab Thickness on Adsorption Energies[a]

	1R/3L	1R/4L	2R/4L	3R/4L
F-CH_2O	−3.53 (−3.47)	−3.57 (−3.51)	−3.58 (−3.52)	−3.57 (−3.51)
F-CH_2	−1.95 (−1.94)	−2.03 (−2.02)	−2.05 (−2.04)	−2.04 (−2.03)
OH	−3.42 (−3.31)	−3.44 (−3.33)	−3.46 (−3.35)	−3.46 (−3.35)

[a]In electronvolts, nR/mL, n for relaxed layers, and m for total layers; the ZPE-corrected adsorption energies are given in parentheses.

on transition metal catalysts extremely depend on the affinity of reactants to metals. Furthermore, furfural has an aromatic furan ring and carbonyl group for potential binding to catalyst surfaces. On the Cu surface, for example, furfural is adsorbed by the carbonyl group through the O lone pair of electrons in an η^1(O)-surface mode,[28,29] whereas on group VIII transition metals (Ni, Pd, and Pt), the C═O double bond interacts with the surfaces in an η^2(C,O) mode.[30−33]

Although much work has been done on furfural conversion on different transition metals in experiment and theory, there is no systematic study about the full potential energy surface of the reaction of furfural to 2-methylfuran on the Cu(111) surface theoretically, despite the plentiful experimental studies about furfural conversion using Cu-based catalysts.[28,29,31,34−37] The only theoretical work[38] reported 2-methylfuran formation from the hydrogenation of furfuryl alcohol on the Cu(111) surface. Furfural conversion on Cu/SiO_2 catalyst mainly results in the selective formation of furfuryl alcohol, and only small amount of 2-methylfuran is observed,[28] but raising the reaction temperature increases the yield of 2-methylfuran.[31] Over Cu supported on SBA-15 silica catalyst with 15 wt % Cu after 5 h of time-on-stream at 170 °C,[37] furfural conversion of 54% and furfuryl alcohol selectivity of 95% have been observed. Furthermore, it is found that a high temperature (270 °C) lowers furfural conversion and furfuryl alcohol selectivity, while the selectivity of 2-methylfuran is increased.

In this work, we used the latest PBE-D3 method, including zero-point energy (ZPE) correction, to explore the mechanism of furfural conversion to 2-methylfuran on the Cu(111) surface under the consideration of van der Waals (vdW) interaction. On the basis of the computed thermodynamic and kinetic data, we identified the possible optimal reaction path and the rate-determining step as well as the rationalized selective formation of furfuryl alcohol and the equilibrium of furfural/furfuryl alcohol conversion under hydrogen-rich conditions. It is also proposed that H_2O might suppress furfural conversion. Our results provide insights into Cu-catalyzed furfural selective conversion and broaden our fundamental understanding into deoxygenation reactions involved in the refining of biomass-derived bio-oils.

2. COMPUTATIONAL METHOD AND MODEL

2.1. Background. In recent years, traditional generalized gradient approximation density functional theory (DFT-GGA) methods have become effective tools in inspecting heterogeneous catalytic reaction pathways and the related thermodynamic and kinetic properties.[39−41] However, DFT-GGA methods, which consider only electrostatic forces,[42,43] cannot describe the weak dispersion associated with vdW interaction,[44] which is particularly important for weak interactions between aromatic molecules and group IB metals. For example, Bilić et al.[45] found that PW91 can give a reasonable adsorption configuration of pyridine on Au(111) but underestimates the adsorption energy. Bilić et al.[46] also found that PW91 and PBE underestimate benzene adsorption energies on copper, silver, and gold surfaces. Similar results are found for pyridine adsorption on the Ag(110) and Cu(110) surfaces.[47]

Using Grimme's semiempirical method to consider the long-range dispersion correction for vdW interaction,[48−50] Liu et al.[51] computed furfural adsorption on the face-centered cubic (fcc) Pd(111), Cu(111), and Pt(111) surfaces and found that on Cu(111), not only the adsorption configuration but also the adsorption energy change significantly upon the change from PBE to PBE-D2, and the increase in the adsorption energy is up to 0.83 eV in magnitude. Moreover, Vorotnikov et al.[30] used the latest PBE-D3 method to investigate the conversion of furfural to furan, furfuryl alcohol, and 2-methylfuran on the Pd(111) surface. Most recently, Wang et al.[52] used PBE-D3 to investigate the coverage-dependent selectivity of furfural conversion on the Pd(111) surface. All these studies revealed that PBE-D3 can reasonably predict not only the adsorption configurations but also the adsorption energies in furfural conversion. Therefore, we used PBE-D3 to compute the full potential energy surface of furfural conversion on the Cu(111) surface. This is the first theoretical study presenting both thermodynamic and kinetic parameters of furfural transformation on the Cu(111) surface.

2.2. Method. All calculations were performed by using the plane-wave-based periodic DFT method implemented in the Vienna ab initio simulation package (VASP, version 5.3.5),[53,54] where the ionic cores are described by the projector augmented wave (PAW) method.[55,56] The exchange and correlation energies were computed using the Perdew, Burke, and Ernzerhof functional with the latest dispersion correction (PBE-D3).[49,50,57] To have accurate energies with errors of <1 meV/atom, a cutoff energy of 400 eV and the Gaussian electron smearing method with σ = 0.20 eV were used. The geometry optimization was converged until all forces acting on the atoms were smaller than 0.02 eV/Å, whereas the energy threshold-defining self-consistency of the electron density was set to 10^{-4} eV. All transition state structures were located using the climbing image nudged elastic band (CI-NEB) method.[58] For each optimized stationary point, we carried out vibrational analysis at the same level of theory to determine its nature (either minimum or saddle point) and ZPE and ensured that each transition state had only one imaginary frequency along the reaction coordinate. For the bulk optimization, the lattice parameter was optimized using the fcc unit cell, and its reciprocal space was sampled with a 15 × 15 × 15 k-point grid generated automatically by using the Monkhorst−Pack method.[59] The optimized lattice parameter of 3.561 Å is close to the experimental value (3.614 Å[60]) and in good agreement with other DFT calculations.[51,61]

2.3. Model. Johnson[62] found that the (111) surface is often exposed in fcc and hexagonal close-packed (hcp) metals, and other surfaces tend to become (111) in crystal growth, crystal surface dissociation, and chemical erosion. Among the low-index surfaces, the Cu(111) surface is found to have the lowest surface energy and represents the most stable surface.[63−66] Hence, we used the Cu(111) surface to execute our study. A vacuum of 15.0 Å was used between the slabs and their periodic images to avoid perpendicular interaction. The surface structural relaxation and

DOI: 10.1021/acscatal.5b00303
ACS Catal. 2015, 5, 4020−4032

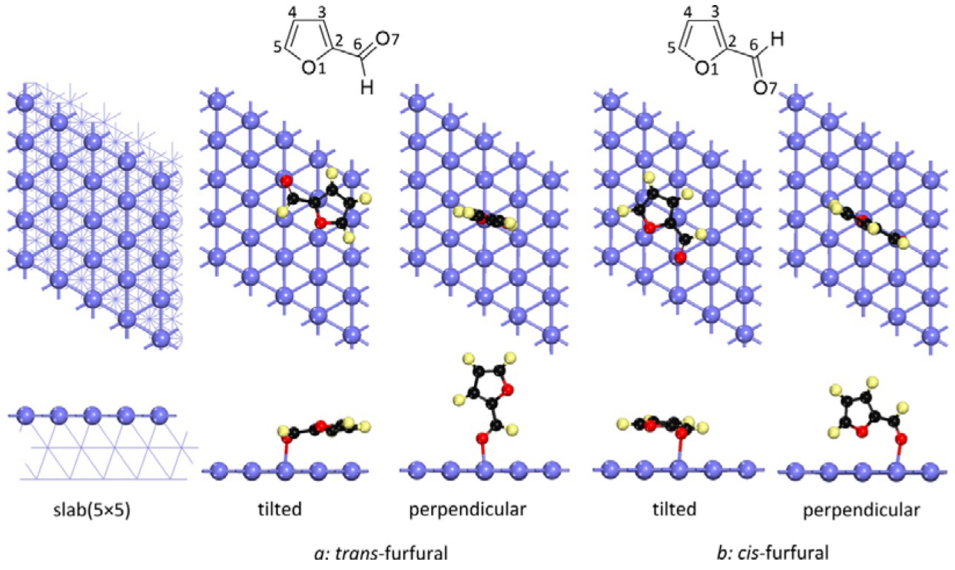

Figure 1. Top (above) and side (below) views of the Cu(111) surface structure and possible adsorption sites: top (t), bridge (b), 3-fold hollow face-centered cubic site (fcc, over a third layer atom), and hexagonal-close-packed site (hcp, over a second layer atom), as well as furfural adsorption (surface/blue, carbon/black, hydrogen/yellow, oxygen/red).

the total energy calculation were performed with the 3 × 3 × 1 Monkhorst−Pack *k*-point sampling. To check the influence of the slab thickness on the adsorption energies, we tested two $p(5 \times 5)$ slab models in different thicknesses in varying the relaxed surface layers. The first slab model has three layers (a total of 75 Cu atoms), and the first layer is allowed to relax; the bottom two layers are fixed to the bulk positions by keeping their optimized lattice constants (1R/3L). The second slab model has four layers (a total of 100 Cu atoms), and the top one, top two, and top three layers are relaxed, respectively, and the corresponding bottom layers are fixed (1R/4L, 2R/4L, 3R/4L, respectively). Using these slab models, we computed the adsorption energies of the most important surface species, 2-furanylmethoxyl (F-CH_2O), 2-furanylmethyl (F-CH_2), and hydroxyl (OH). As shown in Table 1, the computed adsorption energies by using the thick four-layer model are nearly independent of the number of the relaxed layers. The computed adsorption energies by using the thin three-layer model (1R/3L) are close to those by using the thick four-layer model (3R/4L). For example, the adsorption energy for F-CH_2O is −3.47 and −3.51 eV by using the 1R/3L and 3R/4L models, respectively, and the deviation is <2%. For F-CH_2, the adsorption energy is −1.94 and −2.03 eV using the 1R/3L and 3R/4L models, respectively, and the deviation is <5%. For OH, the adsorption energy is −3.31 and −3.35 eV using the 1R/3L and 3R/4L models, respectively, and the deviation is <2%. On the basis of these agreements between the thin and thick models, we wished to use the 1R/3L thin model for computing the potential energy surfaces of furfural hydrogenation conversion. It is also found that ZPE correction has negligible effect on the computed adsorption energies: the largest effect is found for OH (−3.42 vs −3.31 eV), and the smallest effect is found for F-CH_2 (−1.95 vs −1.94 eV).

For the relevant gas phase species, we used a cubic box with side length of 15 Å to calculate the structures and total energies. The geometry optimization was performed until all forces acting on the atoms were smaller than 0.02 eV/Å and the energy difference was lower than 10^{-4} eV.

Surface adsorption takes place on the topmost layer of the slab. All adsorbed species were allowed to relax to their optimized positions. The adsorption energy, E_{ads}, was calculated according to eq 1, in which $E_{X/slab}$ is the total energy of the slab with adsorbed species in its equilibrium geometry, E_{slab} is the total energy of the slab, and E_X is the energy of the free adsorbates in gas phase. Therefore, the more negative the E_{ads}, the stronger the adsorption. All energetic data include ZPE correction, and those without ZPE correction are provided for comparison. It shows clearly that ZPE correction has a negligible effect on the computed kinetic and thermodynamic data; this is the same as found for reactions on iron surfaces[67,68] and iron carbide surfaces.[69]

$$E_{ads} = E_{X/slab} - E_{slab} - E_X \quad (1)$$

The activation energy barrier (E_a) and reaction energy (E_r) were calculated by using eqs 2 and 3, where E_{IS}, E_{TS}, and E_{FS} are the energies of the corresponding initial state (IS), transition state (TS), and the final state (FS), respectively.

$$E_a = E_{TS} - E_{IS} \quad (2)$$

$$E_r = E_{FS} - E_{IS} \quad (3)$$

3. RESULTS AND DISCUSSION

3.1. Adsorption of Intermediates. The top and side reviews of the Cu(111) surface are shown in Figure 1. There are four potential exposed sites for adsorption, i.e.; top (t), bridge (b), 3-fold face-centered cubic site (fcc) over a third layer atom, and 3-fold hexagonal close-packed site (hcp) over a second layer atom.

(a). Adsorption of Furfural, Furfuryl Alcohol and 2-Methylfuran. Furfural (F-CHO) has both *cis* and *trans* configurations, and the *trans* one is slightly more stable than the *cis* one by 0.02 eV, in agreement with the previous theoretical results[51] and experimental findings from IR and Raman spectroscopy studies.[70] We have calculated the adsorption of *cis*- and *trans*-furfural on the Cu(111) surface and found two types of stable adsorption configurations: (i) tilted adsorption, in which the furfural molecule is adsorbed in a tilted position by the interaction between the C═O double bond and the surface; (ii)

DOI: 10.1021/acscatal.5b00303
ACS Catal. 2015, 5, 4020−4032

Table 2. Adsorption Energies E_{ads} (eV) and Bond Distances (Å) of *trans*- and *cis*-Furfural As Well As Furfuryl Alcohol and 2-Methylfuran on the Cu(111) Surface

configuration	E_{ads}	d_{Cu-O}	exp[28]
trans tilted	−0.91/−0.93[a] (−0.90/PBE-D2;[51] −0.07/PBE;[51] −0.16/PBE)	2.161 (2.16/PBE-D2;[51] 2.20/PBE;[51] 2.256/PBE)	−0.53
trans perpendicular	−0.64/−0.63[a] (−0.30/PBE)	2.045 (2.087/PBE)	
cis tilted	−0.88/−0.89[a] (−0.19/PBE)	2.259 (2.248/PBE)	
cis perpendicular	−0.74/−0.72[a] (−0.17/PBE;[28] −0.24/PBE)	2.107,2.638 [(2.05, 3.08)/PBE;[28] (2.174, 2.860)/PBE]	
furfuryl alcohol	−0.97/−0.96[a] (−1.10/PBE-D2;[51] −0.15/PBE;[51] −0.16/PBE)	2.381 (2.25/PBE-D2;[51] 2.35/PBE[51])	−0.30
2-methylfuran	−0.92/−0.93[a] (−0.19/PBE)		−0.16

[a]Values including ZPE correction.

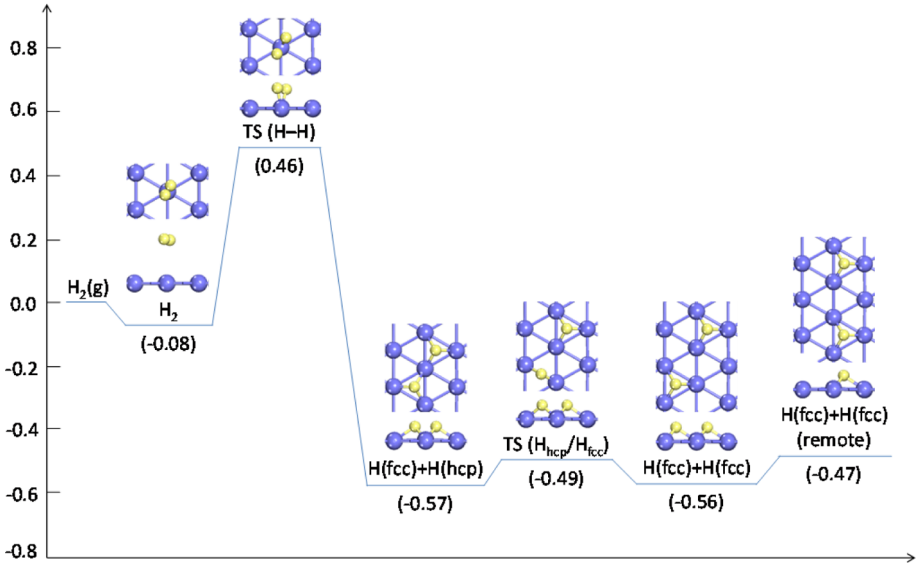

Figure 2. Potential energy surface of H_2 dissociative adsorption and H diffusion (energy is in eV; copper/blue, hydrogen/yellow).

perpendicular adsorption, in which the furfural molecule is almost vertical to the surface with the O atom of the C═O group interacting with surface Cu atom. The adsorption configurations and their structural properties are listed in Figure 1 and Table 2, respectively. As shown in Table 2, the contribution of ZPE correction to the adsorption energies is very small; and the maximal change is only 0.02 eV.

In the tilted adsorption configuration, the O7 atom of the C═O group is in contact with the top site of one surface Cu atom; the Cu−O7 distance is 2.161 Å; and the C6 atom is over the fcc site of the surface with Cu−C6 distances of 2.821, 2.916, and 3.029 Å, as well as the Cu−O7−C6 angle of 108.0°, indicating a nonparallel adsorption. In addition, the Cu−O7−C6−C2 dihedral angle of 94.4° indicates that the furan ring is tilted away from the surface. The computed adsorption energy (−0.93 eV) is in agreement with the reported value (−0.90 eV) by using PBE-D2.[51] Apart from this tilted adsorption configuration, we also computed the perpendicular one, in which the furan molecular plane is nearly vertical to the surface. The Cu−O7 distance is 2.045 Å, and the Cu−O7−C6−C2 dihedral angle is 178.0°. However, the perpendicular adsorption configuration is less stable than the tilted one (−0.63 vs −0.93 eV). On the basis of the rather long Cu−C6 distances in the tilted adsorption configuration, it is easy to conclude that it has the η^1(O) surface bonding mode.

In addition, we computed both tilted and perpendicular adsorption configurations for *cis*-furfural; the adsorption energy is −0.89 and −0.72 eV, respectively. In the tilted adsorption configuration, the Cu−O7 distance is 2.259 Å, and the Cu−C6 distances are 2.814, 3.033, and 3.157 Å. The corresponding Cu−O7−C6 angle is 102.6° and the Cu−O7−C6−C2 dihedral angle is 87.4°. In the perpendicular adsorption configuration, the distances of Cu−O7 and Cu−O1 are 2.107 and 2.638 Å, respectively.

As shown in Table 2, the optimized Cu−O distances from PBE to PBE-D3 are very close, but the PBE-D3 adsorption energies are much stronger than those of PBE, indicating the contribution of dispersion correction. On the basis of the experimentally estimated heat of adsorption of furfural (−0.53 eV),[28] the computed adsorption energy is strongly overestimated by PBE-D3 (−0.93 eV) while badly underestimated by PBE (−0.16 eV). The experimental value is curiously just the average value of PBE-D3 and PBE.

Furthermore, we also computed the adsorption structures and energies of furfuryl alcohol (F-CH_2OH) and 2-methylfuran (F-CH_3). For furfuryl alcohol, the most stable adsorption has the oxygen atom of the OH group at the top site with the Cu−O distance of 2.381 Å, and the furan ring is nearly parallel over the surface. For 2-methylfuran, the molecule face covers the surface without direct bonding interaction, and the shortest Cu−C4 and Cu−H distances are 2.718 and 2.563 Å, respectively. The computed adsorption energies for furfuryl alcohol and 2-methylfuran are −0.96 and −0.93 eV, respectively, and they are larger than the experimentally estimated heats (−0.30 and −0.16 eV,[28] respectively) of adsorption, indicating the strong overestimations of PBE-D3.

(b). H_2 Dissociative Adsorption. Because H_2 has been used in furfural conversion, we computed the H_2 dissociative adsorption

DOI: 10.1021/acscatal.5b00303
ACS Catal. 2015, 5, 4020−4032

on the Cu(111) surface by using PBE-D3. The adsorption configurations and their structural properties are listed in Figure 2 and Table 3, respectively. For the adsorption of H_2 parallel to the surface, the shortest Cu−H distances are 2.960 and 3.022 Å, and the adsorption energy is only −0.08 eV, indicating very weak physisorption. However, the adsorption of two H atoms is much stronger, and the most stable coadsorption configuration has one H atom at the fcc site and the other at the hcp site. Most importantly, they share one surface Cu atom with the distance between two H atoms of 2.957 Å, and the corresponding Cu−H distances are 1.730, 1.737, and 1.745 Å as well as 1.735, 1.737, and 1.745 Å, respectively. The dissociative adsorption energy of H_2 is −0.57 eV, indicating a thermodynamically favorable process. This computed dissociative adsorption energy agrees very well with the experimentally determined heat of adsorption on Cu/SiO_2 catalyst (−0.60 eV[28]), on supported Cu catalysts (−0.56 ± 0.31 eV;[71] −0.58 eV[72]), and on Cu polycrystalline (−0.62 ± 0.06 eV[73]) as well as on other types of copper catalysts.[74]

Table 3. H_2 Dissociation Barrier (E_a/eV) and Energy (E_r/eV) As Well As Critical Bond Distances (Å) in the Transition State

E_a	E_r	d_{H-H}	d_{Cu-H}
0.59/0.54[a]	−0.55/−0.49[a]	1.288	1.548, 1.562
0.5/PW91[75]	−0.2/PW91[75]	1.1/PW91[75]	
0.54/PW91[76]	−0.31/PW91[76]		
0.54/PW91[77]	−0.53/PW91[77]	1.02/PW91[77]	

[a]Values including ZPE correction.

In the transition state TS(H−H), both H atoms are at the top site with the H−H distance of 1.288 Å, and the Cu−H distances are 1.548 and 1.562 Å. The computed H_2 dissociation barrier is 0.54 eV, in agreement with the reported values of about 0.5 eV using PW91 (Table 3).[75−77] Furthermore, we also computed the diffusion ability of H atom on the surface, and the computed diffusion barrier from one hcp site to the next fcc site is only 0.08 eV, which is in close agreement with the previous study (0.14 eV),[78] indicating the high mobility. At such very low coverage, it is also found that the remote coadsorption of two H atoms is 0.10 eV less stable than the one in which both H atoms share one Cu atom (Figure 2).

For the adsorption of one H atom, the structural properties are listed in Table 4. The adsorption energies at the fcc and hcp sites are very close (−2.55 and −2.54 eV), in agreement with the experimental value (−2.43 eV)[79] as well as the reported results (−2.43 and −2.42 eV).[80] It is also noted that the PBE computed adsorption energies of −2.42 and −2.43 eV are closer to the experimental value than those of PBE-D3, indicating negligible dispersion correction.

Table 4. Adsorption Energies E_{ads} (eV) and Bond Distances (Å) of H Atom on the Cu(111) Surface

E_{ads}	d_{Cu-H}	exptl
H at the fcc Site		
−2.55 (−0.33[a]; −0.31[b])	1.743, 1.743, 1.752	−2.43[79]
−2.55/PW91[77]	1.75/PW91[77]	
−2.43/PBE[80]	1.78/PBE[80]	
(−0.34[a]/PW91[78])		
H at the hcp Site		
−2.54 (−0.32[a]; −0.30[b])	1.744, 1.746, 1.750	
−2.55/PW91[77]	1.75/PW91[77]	
−2.42/PBE[80]		
(−0.33[a]/PW91[78])		

[a]Related to gaseous H_2. [b]Values including ZPE correction.

(c). H_2O Dissociative Adsorption. Because H_2O is a principal product from furfural hydrogenation, we computed H_2O dissociative adsorption using PBE-D3 for direct comparison with the available results.[77,78,81−84] The adsorption configurations and their structural properties are listed in Figure 3 and Table 5, respectively. Actually, we can use the reverse reaction for discussing H_2O formation in furfural conversion.

It is found that H_2O has a flat adsorption configuration at the top site, with the Cu−O distance of 2.297 Å and an adsorption energy of −0.32 eV, in perfect agreement with the experimental value (−0.35 eV)[85] and larger than the reported results by using PW91 (−0.21,[78] −0.19,[82] −0.24,[83] and −0.18 eV[84]) without dispersion correction. However, it is also noted that the experimentally determined heat of adsorption of H_2O on the Cu/SiO_2 catalyst (−0.54 eV[28]) is larger than the PBE-D3 value, and this might apparently be due to the additional interaction of H_2O with the support.

The most stable coadsorption configurations of O and OH are located at the neighboring fcc sites, in agreement with the previous studies. The adsorption energies of OH and O (to gaseous O_2) are −3.31 and −1.66 eV, respectively, in close agreement with the reported results (−3.18 and −1.94 eV, respectively).[78]

On the basis of the H_2O adsorption configuration, we computed its dissociation, which has a barrier of 1.28 eV and is slightly endothermic by 0.02 eV. In the transition state TS(HO−H), both dissociating HO and H are still over the top site, with Cu−O and Cu−H distances of 2.044 and 1.679 Å, and the breaking O−H distance is 1.597 Å. In the dissociated state (HO + H), both OH and H are located at the fcc sites, and they share one surface Cu atom. Such coadsorption is less stable than the remote coadsorption by 0.06 eV.

On the basis of the stably remote OH and H coadsorption configuration with OH vertically located at the fcc site, we computed OH dissociation, which has a barrier of 1.64 eV and is endothermic by 0.75 eV, indicating that OH dissociation is neither kinetically nor thermodynamically favorable. In the transition state TS(O−H), the dissociating O is still over the fcc site, with Cu−O distances of 2.017, 1.933, and 1.939 Å, and the H atom moves to the top site with the Cu−H distance of 1.576 Å; the breaking O−H distance is 1.674 Å. In the dissociated state (O + H), both O and H are located at the fcc sites, and they also share one surface Cu atom. Such coadsorption is less stable than the remote coadsorption by 0.10 eV. Because H_2 has a dissociative adsorption energy of −0.57 eV and dissociation barrier of 0.54 eV, the two H atoms from H_2O dissociation will stay stably on the surface rather than show recombinative desorption with a very high barrier of ∼1.04 eV. With respect to the gaseous H_2O molecule, the formation of adsorbed surface O and gaseous H_2 is endothermic by 0.76 eV.

3.2. Mechanism of *trans*-Furfural Conversion to 2-Methylfuran. On the basis of the most stable adsorbed *trans*-furfural in the tilted configuration, we computed the full potential energy surface of furfural (F-CHO) conversion to furfuryl alcohol (F-CH_2OH) and subsequently to 2-methylfuran (F-CH_3). As shown in Scheme 1, the conversion of F-CHO to F-CH_3 can be largely conducted through four competitive pathways (R1 and R2 as well as R3 and R4) and therefore is very complex. Because the H atom has close adsorption energy at

DOI: 10.1021/acscatal.5b00303
ACS Catal. 2015, 5, 4020−4032

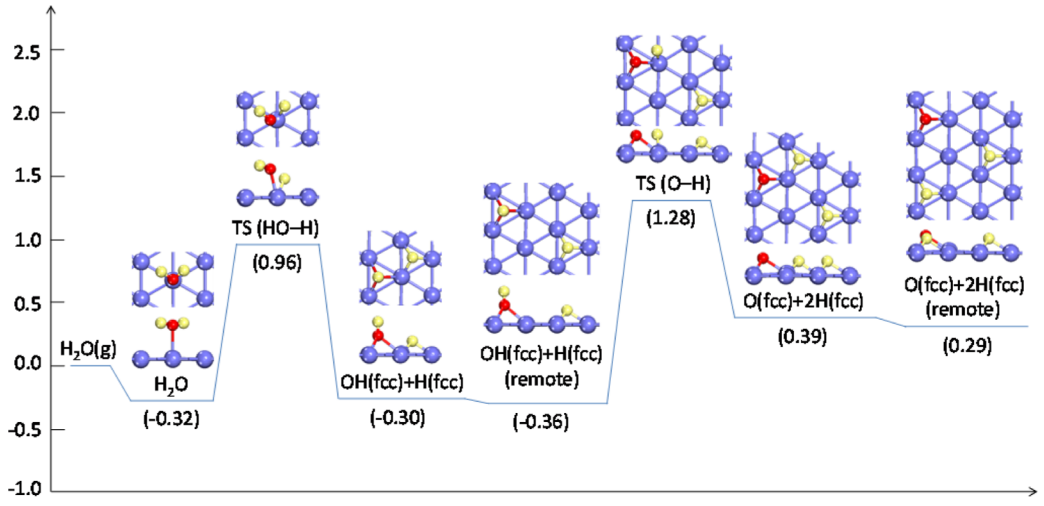

Figure 3. Potential energy surface of H_2O dissociative adsorption (energy is in eV; copper/blue, hydrogen/yellow, oxygen/red).

Table 5. H_2O Stepwise Dissociation Barrier (E_a/eV), Dissociation Energies (E_r/eV) and Critical Bond Distance (d_{O-H}/Å)

E_a	E_r	d_{O-H}
	$H_2O \rightarrow TS(HO-H) \rightarrow OH + H$	
1.50 (1.28[b])/PBE-D3	0.14 (0.02[b]; 0.08[a]/−0.04[a,b]/PBE-D3)	1.597/PBE-D3
1.36/PW91[77]	0.37 (0.01[a])/PW91[77]	2.23/PW91[77]
1.01/PW91[78]	−0.12 (−0.23[a])/PW91[78]	1.59/PW91[78]
1.40/PBE[81]	0.26/PBE[81]	1.67/PBE[81]
1.01/PBE[83]	0.34/PBE[83]	
1.34/PW91[84]	0.35 (−0.01[a])/PW91[84]	
	$OH \rightarrow TS(O-H) \rightarrow O + H$	
1.83 (1.64[b])/PBE-D3	0.85 (0.75[b]; 0.75[a]/0.65[a,b]/PBE-D3)	1.674/PBE-D3
1.76/PW91[77]	1.06 (0.48[a])/PW91[77]	1.61/PW91[77]
1.51/PW91[78]	0.55 (0.37[a])/PW91[78]	1.52/PW91[78]
1.78/PBE[83]	0.65/PBE[83]	
1.76/PW91[84]	1.06 (0.48[a])/PW91[84]	

[a]Dissociation energies related to remote coadsorption are given in parentheses. [b]Values including ZPE correction.

Scheme 1. Potential Reaction Pathways of Furfural Conversion to 2-Methylfuran

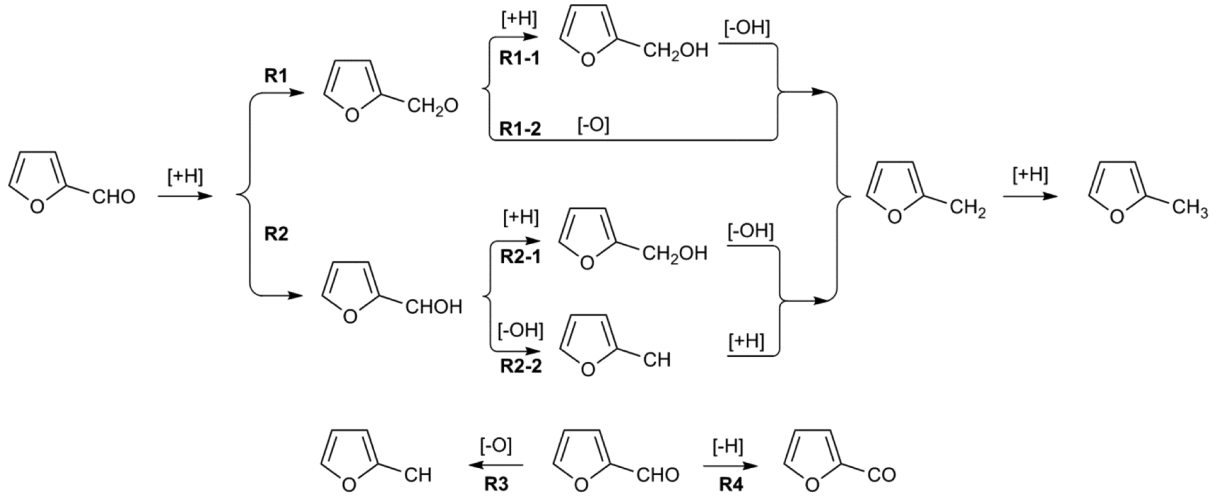

fcc and hcp sites and also high diffusion mobility, we put H to either the fcc or the hcp site, which is close to the substrates for searching the transition state. For exploring the full potential energy surface, however, the computed energy barrier and reaction energy, including ZPE correction, are based on the stable species without direct coadsorption interactions. The selected structural parameters of the initial state (IS), transition state (TS), and the final state (FS) are given in the Supporting Information. It shows that ZPE correction does not affect the free energy barriers and reaction free energies significantly, and qualitatively, both sets of data show the same trend (Supporting Information).

DOI: 10.1021/acscatal.5b00303
ACS Catal. 2015, 5, 4020−4032

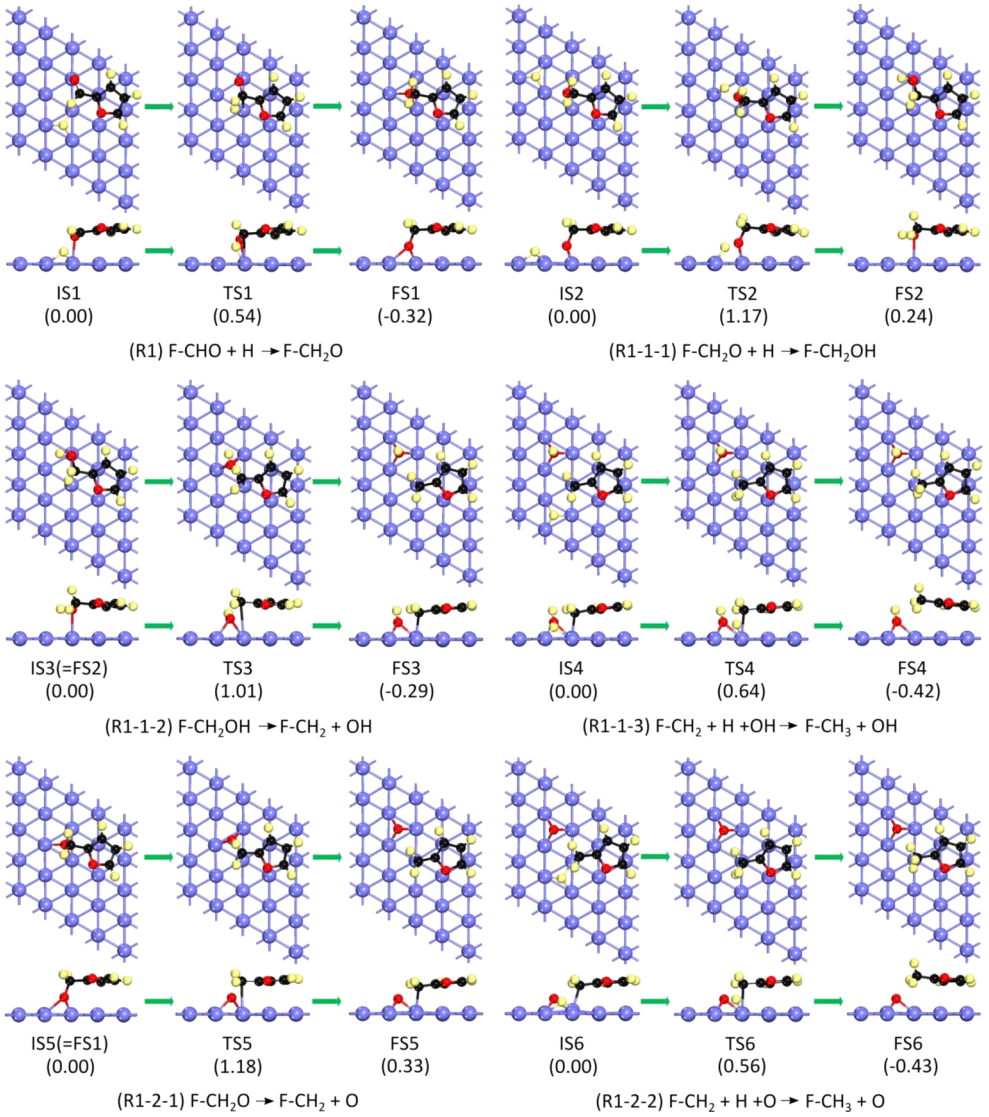

Figure 4. Top (above) and side (below) views of all the optimized geometries for the reaction route R1 (surface/blue, carbon/black, hydrogen/yellow, oxygen/red; F represents the furan ring).

(a). The R1 Route. The first reaction route begins with hydrogen addition to the carbon atom of the C═O group, leading to the alkoxyl intermediate (R1, F-CHO + H → F-CH_2O). The formed F-CH_2O can either be hydrogenated to furfuryl alcohol (R1-1, F-CH_2OH) or dissociate directly into surface alkyl (F-CH_2) and O atom (R1-2, F-CH_2 + O). The formed F-CH_2OH can further either dissociate directly into F-CH_2 and OH (R1-1-2a, F-CH_2OH → F-CH_2 + OH) or be hydrogenolyzed into F-CH_2 and H_2O (R1-1-2b, F-CH_2OH + H → F-CH_2 + H_2O). The overall formed F-CH_2 as well as O or OH groups can be hydrogenated to F-CH_3 and H_2O. On the basis of the most stable tilted adsorption, we computed the coadsorption of F-CHO and H atom. The optimized structures of the adsorbed intermediates are given in Figure 4.

In the coadsorbed structure (IS1), the H atom is located at the hcp site. In the transition state (TS1), the forming C6−H distance is 1.657 Å. In the F-CH_2O (FS1), the adsorption of the O7 atom is at the hcp site with Cu−O7 distances of 2.030, 2.166, and 2.021 Å. The computed barrier is 0.54 eV, in close agreement with the available data (0.56 and 0.46 eV[51]). The reaction is exothermic by 0.32 eV.

For the formation of F-CH_2OH (FS2) along R1-1, we calculated the coadsorption geometry of the H atom and F-CH_2O (IS2), where the H atom is at the hcp site, and the O7 atom is at the bridge site. In the transition state (TS2), the forming O7−H distance is 1.360 Å, and the H atom moves to the top site with the Cu−H distance of 1.709 Å. The O7 atom is at the bridge site with Cu−O7 distances of 2.219 and 2.031 Å. The computed barrier is 1.17 eV, in close agreement with the available values (1.15 and 1.12 eV[51]). The reaction is endothermic by 0.24 eV. It is noted that for the adsorption of F-CH_2OH, the adsorption configuration in FS2 is the most stable and has the O7 atom at the top site with the Cu−O7 distance of 2.381 Å.

Following the R1-1 route, the next step is the dehydroxylation of F-CH_2OH to F-CH_2 and OH (R1-1-2a). On the basis of the most stable adsorption configuration of F-CH_2OH (IS3 = FS2), we computed the dissociation transition state (TS3) and products (FS3). In TS3, the OH group is shifted to the bridge site with Cu−O7 distances of 2.141 and 2.052 Å, and the breaking C6−O7 distance is 1.955 Å. In FS3, the OH group is vertically located at the fcc site with Cu−O7 distances of 2.046, 2.016, and 2.068 Å, and the formed F-CH_2 is located at the top

DOI: 10.1021/acscatal.5b00303
ACS Catal. 2015, 5, 4020−4032

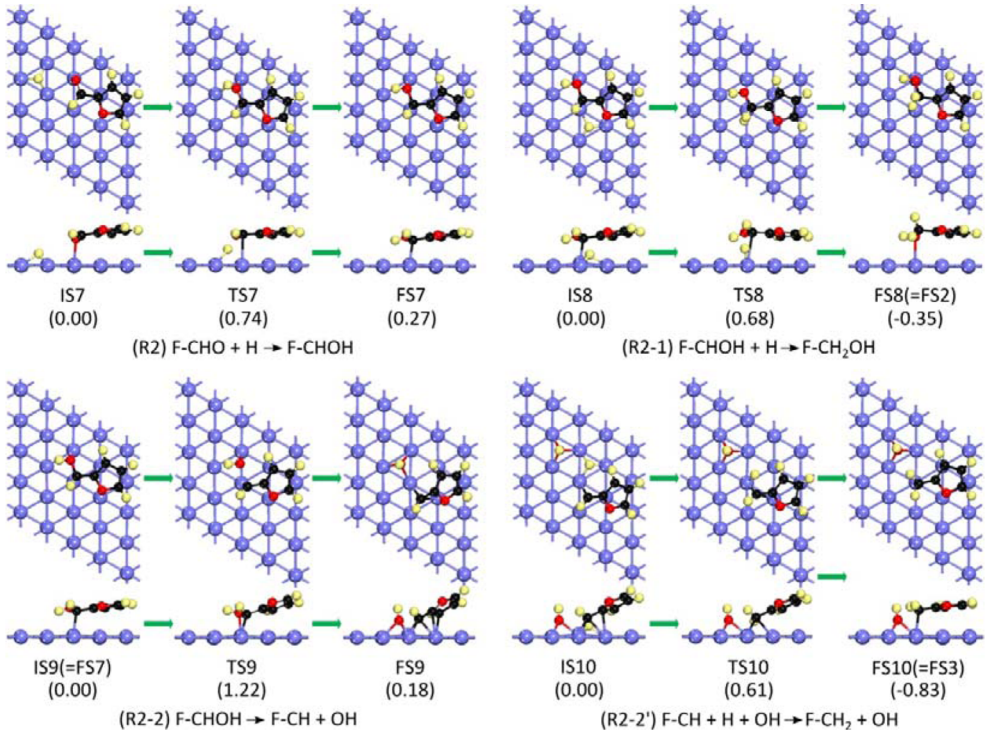

Figure 5. Top (above) and side (below) views of all the optimized geometries for the reaction route R2 (surface/blue, carbon/black, hydrogen/yellow, oxygen/red; F represents the furan ring).

site via the C6 atom with the Cu−C6 distance of 2.082 Å. The computed energy barrier is 1.01 eV, and the reaction is exothermic by 0.29 eV. In addition, we also tried intensively to obtain the hydrogenolysis step (R1-1-2b) on the basis of a coadsorbed state of F-CH_2OH and H; however, we could not find any reasonable transition states. Those with very long C−O and very short O−H distances as well as very short C−O and very long O−H distances are very high in energy; therefore, the hydrogenolysis step of F-CH_2OH has been excluded. In contrast, Xia et al.[38] reported the H-assisted F-CH_2OH dissociation into F-CH_2 (F-CH_2OH + H → F-CH_2 + H_2O) and found a very low barrier for the reaction (0.11 eV). However, this result is questionable because they did not use the coadsorbed F-CH_2OH and H as the initial state; instead, they used F-CH_2−OH_2 as the initial state, where the O−H bond is already formed (1.004 Å), and this explains why the reaction barrier is very low.

The last step is the formation of F-CH_3 (R1-1-3) starting from the coadsorbed F-CH_2, OH and H as the initial state. In the most stable coadsorption configuration (IS4), there are practically no changes for the coadsorption of OH and F-CH_2 (FS3), and the H atom is located at the fcc site. In the transition state (TS4), the H atom goes to the top site with the Cu−H distance of 1.619 Å, and the forming C6−H distance is 1.639 Å. In the final state (FS4), the OH is still vertically located at the fcc site. The computed energy barrier is 0.64 eV, and the reaction is exothermic by 0.42 eV. The parallel and competitive route to R1-1-3 is H_2O formation from the coadsorbed F-CH_2, OH, and H. In the transition state [TS(HO−H)], the H atom and OH group move from the fcc sites to the top sites with Cu−O7 and Cu−H distances of 2.051 and 1.747 Å, and the forming O7−H distance is 1.578 Å. The computed reaction barrier is 1.07 eV, and the reaction is slightly endothermic by 0.04 eV. Compared with the hydrogenation of F-CH_2 leading to F-CH_3, H_2O formation is neither kinetically (1.07 vs 0.64 eV) nor thermodynamically (0.04 vs −0.42 eV) favorable.

On the coadsorbed state of F-CH_3, OH, and H, we computed H_2O formation. In the transition state [TS(HO−H)′], both the H atom and OH group move from the fcc sites to the top sites, and the bond distances of Cu−O7 and Cu−H are 2.033 and 1.778 Å, respectively. In addition, the forming O7−H distance is 1.531 Å. The computed barrier is 1.20 eV, and the reaction is slightly endothermic by 0.10 eV. These values are close to those (1.32 vs 0.04 eV) on the clean surface, as shown in Figure 3, indicating that H_2O formation should be not competitive, and F-CH_3 formation is favorable both kinetically and thermodynamically. For F-CH_3, the molecule face covers the surface without direct bonding interaction, and this is the same as found on the clean surface.

The alternative way to R1-1 is the dissociation of F-CH_2O into F-CH_2 and O (R1-2). Starting from the initial state (IS5 = FS1), we computed the transition state (TS5) in which the O7 atom is moved to the bridge site with Cu−O7 bond distances of 1.925 and 1.951 Å, and the breaking C6−O7 distance is 1.910 Å. The F-CH_2 group is nearly parallel to the surface, and the C6 atom is located at the top site with the Cu−C6 distance of 2.736 Å. In the final state (FS5), the O7 atom is located at the fcc site with Cu−O7 distances of 1.902, 1.901, and 1.908 Å, and the F-CH_2 species is adsorbed at the top site through the C6 atom with the Cu−C6 distance of 2.083 Å, which is almost the same as that (2.082 Å) of FS3. The computed energy barrier is 1.18 eV, and the reaction is endothermic by 0.33 eV. Compared with the H addition step (F-CH_2O + H → F-CH_2OH), this dissociation is less favored thermodynamically by 0.09 eV, although both steps have very close energy barriers (1.17 vs 1.18 eV). Therefore, F-CH_2O dissociation and hydrogenation should be competitive.

The subsequent step is the formation of F-CH_3, starting from the coadsorbed O, F-CH_2 and H (IS6), where the coadsorbed O

DOI: 10.1021/acscatal.5b00303
ACS Catal. 2015, 5, 4020−4032

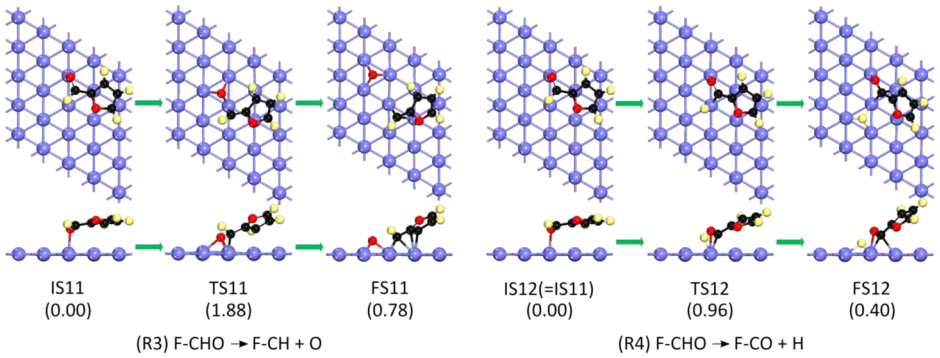

Figure 6. Top (above) and side (below) views of the optimized geometries for the reaction routes R3 and R4 (surface/blue, carbon/black, hydrogen/yellow, oxygen/red; F represents the furan ring).

and F-CH_2 are nearly the same as found in FS5, and the H atom is located at the fcc site. In the transition state (TS6), the H atom goes to the top site with the Cu−H distance of 1.630 Å, and the forming C6−H distance is 1.669 Å. At the same time, the Cu−C6 distance is elongated from 2.088 to 2.400 Å. In the final state (FS6), the remaining O6 atom is still located at the fcc site, and F-CH_3 is over the surface. The computed barrier is 0.56 eV, and the reaction is exothermic by 0.43 eV, which is similar to the R1-1-3 step (0.64 vs −0.42 eV). The parallel and competitive route to R1-2-2 is the formation of OH from the coadsorbed F-CH_2, O, and H. In the transition state [TS(O−H)], the O7 atom is still at the fcc site with Cu−O7 distances of 1.958, 1.948, and 2.030 Å, while the H atom moves to the top site with the Cu−H distance of 1.536 Å, and the forming O7−H distance is 1.633 Å. The computed barrier is 0.95 eV, and the reaction is exothermic by 0.38 eV. Compared with the hydrogenation of F-CH_2 leading to F-CH_3, OH formation is less favorable kinetically by 0.39 eV, although both steps have very close reaction energies (−0.38 vs −0.43 eV).

On the coadsorbed state of F-CH_3, O, and H, we computed the formation of OH. In the transition state [TS(O−H)′], the O7 atom is still at the fcc site with Cu−O7 distances of 1.953, 1.992, 2.030 Å, while the H atom moves to the top site with the Cu−H distance of 1.635 Å, and the forming O7−H distance is 1.557 Å. The computed barrier is 1.03 eV, and the reaction is exothermic by 0.37 eV. These values are close to those (0.99 vs −0.65 eV) on the clean surface (Figure 3). Considering the high barriers (1.03 and 1.20 eV, respectively) of OH and H_2O formations, F-CH_3 formation is favorable both kinetically and thermodynamically.

(b). The R2 route. The alternative reaction route starts with the formation of 2-furanyl(hydroxy)methyl (R2, F-CHOH), which can be either hydrogenated into F-CH_2OH (R2-1) or dehydroxylated into 2-furanylmethylene (F-CH) and OH (R2-2). The formed F-CH_2OH can further dissociate into F-CH_2 and OH (R1-1-2), and the formed F-CH can be hydrogenated into F-CH_2 (R2-2′). The final formation of F-CH_3 and H_2O completes the reaction. The optimized structures are given in Figure 5.

On the basis of the stable adsorption configuration of F-CHO and H atom (IS7), the H atom is located at the fcc site, which is close to the O7 atom of the carbonyl group. As found in IS1, the O7 atom is located at the top site. In the transition state (TS7), the C6═O7 bond length increases from 1.262 to 1.290 Å, and the forming O7−H distance is 1.411 Å. The H atom goes from the fcc site to the top site with the Cu−H distance of 1.813 Å, and the C6 atom is located at the top site with the Cu−C6 distance of 2.673 Å as well as the shortest Cu−O7 distance is 2.680 Å. In the final state (FS7), the C6 atom of the hydroxyl−alkyl group (F-CHOH) is located at the top site with the Cu−C6 distance of 2.097 Å. The computed barrier is 0.74 eV, in agreement with the reported data (0.74 and 0.71 eV[51]), and the reaction is endothermic by 0.27 eV. Compared with the R1 step, H addition to the O7 atom is neither kinetically (0.74 vs 0.54 eV) nor thermodynamically (0.27 vs −0.32 eV) competitive. Nevertheless, we carried out the subsequent steps for comparison.

The next step is the formation of F-CH_2OH through hydrogen addition (R2-1). In the stable coadsorbed state of F-CHOH and H (IS8), the H atom is located at the fcc site close to the CH group. In the transition state (TS8), the H atom is at the top site with the Cu−H distance of 1.629 Å, the F-CHOH species is roughly parallel to the surface with the shortest Cu−C6 distance of 2.733 Å, and the forming C6−H distance is 1.793 Å. The final state (FS8) is the same as discussed above (FS2). The computed barrier is 0.68 eV, which is higher than the reported value (0.45 eV[51]), and the reaction is exothermic by 0.35 eV. The formation of F-CH_3 and H_2O follows the same way as discussed above. Apart from hydrogen addition, we also computed the corresponding hydrogenolysis step with the formation of F-CH_2 and OH (F-CHOH + H → F-CH_2 + OH); however, the computed barrier is very high (1.43 eV), and the reaction is exothermic by 0.44 eV and, therefore, not favored kinetically with the respect of F-CH_2OH formation (R2-1).

The competitive route to R2-1 is the formation of F-CH through C−O dissociation (R2-2). Starting from the adsorbed F-CHOH (IS9 = FS7), we computed the dissociation transition state (TS9) in which both OH and methylene groups are adsorbed at the top sites with Cu−O7 and Cu−C6 distances of 2.134 and 1.949 Å, respectively, and the breaking C6−O7 distance is 1.965 Å. In the final state (FS9), the formed OH group is located at the fcc site with Cu−O7 distances of 2.003, 2.019, and 2.111 Å, and the C6 atom is located at the fcc site with Cu−C6 distances of 2.060, 2.106, 2.109 Å, while at the same time, the neighboring C2 and C3 atoms of the furan ring also interact with the surface Cu atoms with the Cu−C2 distance of 2.252 Å and the Cu−C3 distance of 2.182 Å. The computed barrier is 1.22 eV, and the reaction is endothermic by 0.18 eV; therefore, this step is also neither kinetically nor thermodynamically competitive with F-CH_2OH formation (R2-1).

For the subsequent formation of F-CH_2 from hydrogen addition to F-CH, we computed the coadsorption of OH, F-CH, and one H atom (IS10) in which the H atom is located at the hcp site close to the methylene carbon atom and the F-CH group has the same adsorption structure as found in FS9. In the transition

DOI: 10.1021/acscatal.5b00303
ACS Catal. 2015, 5, 4020−4032

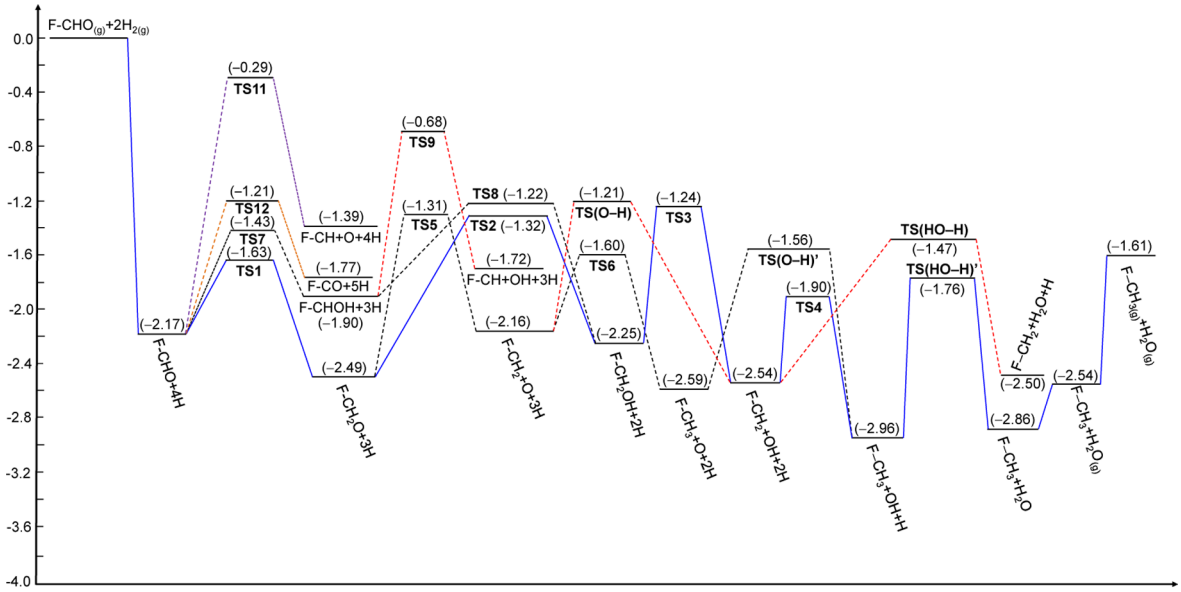

Figure 7. Potential energy surfaces (in eV) for *trans*-furfural conversion to 2-methylfuran on the Cu(111) surface (F represents the furan ring).

state (TS10), the H atom moves to the top site with the Cu−H distance of 1.582 Å, and the C6 atom of the methylene group is at the bridge site with Cu−C6 distances of 1.990 and 2.201 Å while the forming C6−H distance is 1.635 Å. The final state (FS10) is the same as FS3 discussed above. The computed barrier is 0.61 eV, and the reaction is exothermic by 0.83 eV. The parallel and competitive route to R2-2′ is the formation of H_2O from the coadsorbed F-CH, OH, and H. In the transition state [TS(HO-H)″], the H atom and OH group move from the fcc sites to the top sites with Cu−O7 and Cu−H distances of 2.008 and 1.769 Å, and the forming O7−H distance is 1.636 Å. The computed reaction barrier is 1.02 eV, and the reaction is exothermic by 0.14 eV. Compared with the hydrogenation of F-CH leading to F-CH_2, H_2O formation is neither kinetically (1.02 vs 0.61 eV) nor thermodynamically (−0.14 vs −0.83 eV) favorable. The formation of F-CH_3 and H_2O follows the same way as discussed above.

(c). The R3 and R4 Routes. The third and fourth reaction routes start with the direct dissociation of the F-CHO group either into surface O and F-CH (R3) followed by the hydrogenation until the formation of F-CH_3 and H_2O or into F-CO and H (R4), followed by C−O dissociation and stepwise hydrogenation until the formation of F-CH_3 and H_2O. The optimized structures are shown in Figure 6.

Starting from the most stable adsorption of F-CHO (IS11), the dissociation transition state (TS11) and final state (FS11) have been computed. In TS11, the O7 atom is located at the hcp site with Cu−O7 distances of 2.062, 2.019, and 1.943 Å, and the methylene carbon is located approximately at the top site with the Cu−C6 distance of 1.943 Å. The breaking C6−O7 distance is 2.052 Å. In FS11, the oxygen atom is located at the fcc site with Cu−O7 distances of 1.899, 1.901, and 1.902 Å, while the F-CH group is located at the fcc site with the same adsorption configuration as found in FS9. The direct C═O dissociation has a very high barrier of 1.88 eV and is highly endothermic by 0.78 eV.

For the F-CHO dissociation into F-CO and H (R4), we computed the dissociation transition state (TS12) and final state (FS12). In TS12, the H atom is located at the top site with the Cu−H distance of 1.566 Å, and the F-CO species is located approximately at the bridge site with Cu−C6 and Cu−O7 distances of 2.060 and 2.090 Å, respectively. The breaking C6−H distance is 1.771 Å. In FS12, the H atom is located at the hcp site with Cu−H distances of 1.731, 1.723, and 1.743 Å, while the F-CO group is over the fcc site through the CO group with the Cu−O7 distance of 2.112 Å and Cu−C6 distances of 2.047 and 2.174 Å, respectively. The C−H direct dissociation has a barrier of 0.96 eV and is endothermic by 0.40 eV. In comparison with the lower barrier and exothermic reaction energy (0.54 and −0.32 eV, respectively) of F-CH_2O formation from F-CHO hydrogenation in the R1 route, the direct C═O and C−H dissociations in the R3 and R4 routes are not competitive kinetically and thermodynamically on the basis of their higher barriers (1.88 and 0.96 eV, respectively) and endothermic reaction energies (0.78 and 0.40 eV, respectively). Therefore, such direct C═O and C−H dissociations under hydrogenation condition can be ruled out, and we avoided their subsequent reactions.

3.3. Potential Energy Surface. On the basis of the above discussion, we plotted the full potential energy surface, including ZPE correction (Figure 7), on the basis of a step-by-step comparison for general comparison, that is, searching all possible paths for a given adsorbed species obtained from the previous step and continuing only those reaction paths with the lowest reaction barriers while discarding those with obviously higher barriers. Because the direct C═O and C−H dissociations in the R3 and R4 routes have very high barriers (1.88 and 0.96 eV, respectively) and are highly endothermic (0.78 and 0.40 eV, respectively), they are not included in our comparison.

As shown in Figure 7, the first hydrogen addition step toward F-CH_2O formation is more favorable than F-CHOH formation both kinetically (0.54 vs 0.74 eV) and thermodynamically (−0.32 vs 0.27 eV). This clearly shows the preference of F-CH_2O formation. In the subsequent reaction starting from F-CH_2O, hydrogen addition toward F-CH_2OH formation has a barrier of 1.17 eV and is slightly endothermic by 0.24 eV, while the direct C−O dissociation into F-CH_2 and O has a barrier of 1.18 eV and is endothermic by 0.33 eV. This shows that both steps are competitively favorable kinetically and thermodynamically.

DOI: 10.1021/acscatal.5b00303
ACS Catal. 2015, 5, 4020−4032

In the dehydroxylation step of F-CH_2OH, the C−O dissociation has barrier of 1.01 eV and is exothermic by 0.29 eV. From the formed F-CH_2, the formation of F-CH_3 has a barrier of 0.64 eV and is exothermic by 0.42 eV. The final step is the formation of H_2O from the surface OH group. The barrier is 1.20 eV, and the reaction is slightly endothermic by 0.10 eV. The formation of 2-methylfuran from furfural hydrogenation is exothermic (−1.61 eV).

On the basis of these results, it is interesting to discuss the rate-determining step in the whole reactions. As shown in Figure 7, there are two competitive steps (R1-1 and R1-2): F-CH_2OH formation from F-CH_2O hydrogenation and F-CH_2O dissociation. For F-CH_2OH formation, F-CH_2O hydrogenation with the highest barrier (1.17 eV) should be the rate-determining step.

For F-CH_3 formation from F-CH_2O dissociation (F-CH_2O → F-CH_2 + O) and hydrogenation (F-CH_2 + O + 3H → F-CH_3 + O + 2H or F-CH_2 + OH + 2H), F-CH_3 formation and OH formation are parallel and competitive, and H_2O formation is sequential. The barrier of F-CH_2O dissociation is higher than those (1.18 vs 0.56 or 0.95 eV) of the formation of F-CH_3 or OH. In addition, F-CH_2O dissociation is endothermic (0.33 eV), and the formation of F-CH_3 and OH is exothermic (−0.43 and −0.38 eV, respectively). Therefore, F-CH_2O dissociation has the highest barrier and should determine the reaction rate, and the formation of F-CH_3 is more favorable and competitive kinetically and thermodynamically than that of OH. With the coadsorbed F-CH_3, O, and 2H, the subsequent H_2O stepwise formation from O and H as well as from OH and H has barriers of 1.03 and 1.20 eV, respectively. Considering the full reaction, the barrier of F-CH_2O dissociation is comparable with that of H_2O formation. Since the formed F-CH_3 has low adsorption energy and can desorb easily from the surface, the surface will be free of F-CH_3, the barrier of H_2O formation (1.32 eV) on the clean surface should be the upper limit of the whole conversion, and H_2O formation should also be the rate-determining step depending on the reaction conditions. This might explain the observed F-CH_2OH selective formation at low temperature and the increased yield of F-CH_3 at high temperature.

On the basis of the high barrier of H_2O formation from OH and H, we considered the possible OH accumulation and OH disproportionation reaction (2OH → H_2O + O). On the Fe(100) and Fe(110) surfaces with accumulated OH species (high OH coverage), Liu et al.[86,87] reported that OH disproportionation is more favorable kinetically than OH direct hydrogenation, leading to H_2O. On the Cu(111) surface with two coadsorbed OH groups at the neighboring fcc sites, it is found that OH disproportionation has a barrier of only 0.17 eV and is slightly endothermic by 0.06 eV. In the transition state TS(H−OH), one OH group is at the fcc site, the second OH group moves to the top site, and the breaking O−H distance is 1.077 Å, while the forming O−H distance is 1.431 Å. In the final state, the formed H_2O is at the top site and the O atom is at the fcc site. On the basis of this very low barrier of OH disproportionation, it can be concluded that OH accumulation on the Cu(111) surface should be very unlikely. Because OH disproportionation always forms one surface O, the removal of the last surface O should follow the successive hydrogenation step with the formation of H_2O.

For F-CH_3 formation from F-CH_2OH, the highest barrier is found on the step of F-CH_2OH into F-CH_2 and OH (1.01 eV), which is lower than that of H_2O formation from OH and H (1.20 eV). Therefore, H_2O formation should be the rate-determining step in F-CH_2OH conversion to F-CH_3.

It is also interesting to correlate our data with those from experimental studies obtained on a Cu/SiO_2 catalyst at 230−290 °C.[28] A typical transmission electron microscopy (TEM) image of the prepared Cu/SiO_2 catalyst shows a good dispersion of metallic copper clusters with an average particle size of about 3 nm on the silica support after a pretreatment conducted in pure H_2.[28] It is found experimentally that F-CHO and F-CH_2OH can form an equilibrium under hydrogen-rich conditions. Our results (Figure 7) show that the barriers of F-CH_2OH dehydrogenation and dissociation are very close (0.93 vs 1.01 eV), and both steps also have very close reaction energies (−0.24 vs −0.29 eV). This shows a perfect agreement between theory and experiment.

Computationally, we found that F-CH_2O dissociation into F-CH_2 and O has an energy barrier very close to that of F-CH_2O hydrogenation to F-CH_2OH, and F-CH_3 and F-CH_2OH should be formed in close quantities. However, this apparently disagrees with the experimental findings, in which F-CH_2OH is the major product and F-CH_3 is the minor product. Inspections into the experimental condition reveal no disagreement with our computations. This is because a very high H_2/feed ratio (25:1) was used in the experiment, and such a high H_2/feed ratio will shift the reaction to the formation of F-CH_2OH and suppress F-CH_2O dissociation.

It is found experimentally that water can suppress furfural conversion, especially at low temperatures. This finding also agrees with our computed results. As the last step of the conversion (Figure 7), H_2O dissociation and formation have almost the same barriers, and they form an equilibrium. Increasing the H_2O content will shift the reaction toward the formation of the surface OH and H, and such coadsorbed species will block the available surface sites and consequently suppress furfural conversion.

The final issue is the selectivity of furfural conversion mainly to furfuryl alcohol from the hydrogenation of the C═O bond, with only a small amount of 2-methylfutan, obtained from a subsequent C−O cleavage in furfuryl alcohol.[28] On the basis of the potential energy surface, one might conclude that 2-methylfuran should be the only product, since the computed barrier of F-CH_2OH dissociation is even lower than that of F-CH_2O hydrogen addition (1.01 vs 1.17 eV). This disagreement might come from the very strongly overestimated adsorption energy of F-CH_2OH of PBE-D3 in comparison with the available experimentally estimated heat of adsorption (−0.96 vs −0.30 eV). Because of the low heat of adsorption of F-CH_2OH and the high H_2 dissociative adsorption energy (−0.60 eV),[28] the hydrodeoxygenation of F-CH_2OH might not obey the Langmuir−Hinshelwood mechanism. Instead, it might follow the Eley−Rideal mechanism in which F-CH_2OH comes from the gas phase.

It is now interesting to compare our results with those computed on the Pd(111) surface.[30,33,51,88] On Pd(111), F-CHO has a flat adsorption configuration in which both the C═O group and the five-membered aromatic ring bind to the surface, the C═O group is located at the bridge site, and the furan ring is centered at the 3-fold fcc site. This is different from the tilted adsorption of F-CHO on the Cu(111) surface. In addition, the F-CHO adsorption energy (−1.83 eV/PBE-D3[30] and −2.38 eV/PBE-D2[51]) on the Pd(111) surface is much stronger than that on the Cu(111) surface (−0.93 eV/PBE-D3 and −0.90 eV/PBE-D2[51]).

On Pd(111), the thermodynamically favored products are furan and CO, and their formation is exothermic by 1.46 eV, whereas the formation of F-CH_2OH is endothermic by 0.56

DOI: 10.1021/acscatal.5b00303
ACS Catal. 2015, 5, 4020−4032

eV.[30] Therefore, furan should be the principal product, and this is in agreement with the experimental observation.[33] Most recently, Wang et al.[52] used PBE-D3 to investigate the coverage-dependent selectivity of furfural conversion on the Pd(111) surface and found that the hydrogenation selectivity changes with coverage-dependent adsorption configurations.

4. CONCLUSIONS

In this work, we investigated the full potential energy surface of furfural conversion to 2-methylfuran on the Cu(111) surface using density functional theory with the latest correction for the long-range dispersion interaction (PBE-D3). All reported energetic data include ZPE correction. Our goal is the full reaction mechanisms in explaining the experimentally observed selectivity and reactivity as well as the suppressing effect of H_2O in furfural conversion. Our results not only provide the insights into Cu-catalyzed furfural selective conversion but also broaden our fundamental understanding into deoxygenation reactions of oxygenates involved in the refining of biomass-derived oils.

It is first found that long-range dispersion correction overestimates the adsorption energy of furfural (−0.93 vs −0.53 eV), furfuryl alcohol (−0.96 vs −0.30 eV), and 2-methylfuran (−0.93 vs −0.16 eV), whereas those of H_2 (−0.57 vs −0.62 ± 0.06 eV) and H_2O (−0.32 vs −0.35 eV) can be reproduced nearly quantitatively, indicating that it should be critical in discussing the reaction barriers and reaction energies in furfural conversion.

On the basis of our detailed comparisons, the formation of an alkoxyl group from the first H addition is kinetically and thermodynamically more favorable (F-CHO + H → F-CH_2O), and the second H atom addition leading to the formation of furfuryl alcohol is the rate-determining step (F-CH_2O + H → F-CH_2OH). For 2-methylfuran formation from furfuryl alcohol dissociation into surface alkyl and OH groups (F-CH_2OH → F-CH_2 + OH), the successive H_2O formation from surface OH and H is the rate-determining step (OH + H → H_2O). In addition, the formation of 2-methylfuran from the dissociation of the alkoxyl group (F-CH_2O → F-CH_2 + O; F-CH_2 + O → F-CH_3) should be competitive with the formation of furfuryl alcohol. For the selective formation of furfuryl alcohol, hydrogen coverage on the surface should play the decisive role, and the high hydrogen concentration should accelerate F-CH_2O hydrogenation and suppress F-CH_2O dissociation.

The experimentally observed selective formation of F-CH_2OH under hydrogen-rich conditions (H_2/furfural = 25) can be explained on the basis of different reaction mechanisms. Because of the strong and comparable adsorption energies of F-CHO and H_2, F-CH_2OH formation obeys the Langmuir−Hinshelwood mechanism in which the dissociatively adsorbed H atoms and F-CHO can coadsorb onto the surface. Because of the lower adsorption energy of F-CH_2OH, 2-methylfuran formation from F-CH_2OH should follow the Eley−Rideal mechanism with furfuryl alcohol from the gas phase (F-CH_2OH → F-CH_2 + OH; F-CH_2 + H → F-CH_3 and OH + H → H_2O). Both the reaction mechanisms and the proposed rate-determining steps can explain the observed selectivity of F-CH_2OH formation at low temperature and the increased yield of F-CH_3 at high temperature.

The observed equilibrium of F-CHO/F-CH_2OH conversion from F-CH_2OH can be explained by the comparable kinetic and thermodynamic parameters of F-CH_2OH dehydrogenation and dissociation. The observed effect of water suppressing furfural conversion, especially at low temperature, can be explained by the equilibrium of water-dissociative adsorption (H_2O = OH + H), the added H_2O will shift the reaction toward OH and H, and they will block the adsorption sites for furfural conversion. To improve the conversion of furfuryl alcohol to 2-methylfutan, it is also necessary to fine-tune hydrogen coverage on the surface to enable the coadsorption of furfuryl alcohol and hydrogen as well as to remove the formed water from the surface. Despite the fact that our single study is not extensive on the basis of the complex surface structures of catalysts, one can see that it is necessary to modify catalysts to have a higher adsorption ability of furfuryl alcohol as well as a lower adsorption ability of H_2 and H_2O and to accelerate H_2O formation by lowering the barriers.

■ ASSOCIATED CONTENT

Supporting Information

The Supporting Information is available free of charge on the ACS Publications website at DOI: 10.1021/acscatal.5b00303.

Bond distances of the IS, TS, and FS for all the reaction pathways (Table S1); reaction barrier, E_a (eV), and reaction energy, E_r (eV), of all the reaction pathways (Table S2); top and side views of the optimized geometries for the stepwise formation of H_2O (Figure S1); top and side views of the optimized geometries for the disproportionation of OH (Figure S2) (PDF)

■ AUTHOR INFORMATION

Corresponding Author

*E-mail: haijun.jiao@catalysis.de.

Notes

The authors declare no competing financial interest.

■ ACKNOWLEDGMENTS

This work was supported by the Major State Basic Research Development Program of China (973 Program, 2012CB215305) and the Chinese Academy of Science and Synfuels CHINA. Co., Ltd. We also acknowledge general financial support from the BMBF and the state of Mecklenburg-Vorpommern. Y.S. thanks Dr. Rui Gao for help.

■ REFERENCES

(1) Corma, A.; Iborra, S.; Velty, A. *Chem. Rev.* **2007**, *107*, 2411−2502.
(2) Serrano-Ruiz, J. C.; West, R. M.; Dumesic, J. A. *Annu. Rev. Chem. Biomol. Eng.* **2010**, *1*, 79−100.
(3) Werpy, T.; Petersen, G. Top Value Added Chemicals from Biomass. *U.S. Dept. of Energy* **2004**, *1*, 1−76.
(4) Furimsky, E. *Appl. Catal.* **1983**, *6*, 159−164.
(5) West, R. M.; Liu, Z. Y.; Peter, M.; Gärtner, C. A.; Dumesic, J. A. *J. Mol. Catal. A: Chem.* **2008**, *296*, 18−27.
(6) Huber, G. W.; Chheda, J. N.; Barrett, C. J.; Dumesic, J. A. *Science* **2005**, *308*, 1446−1450.
(7) Román-Leshkov, Y.; Barrett, C. J.; Liu, Z. Y.; Dumesic, J. A. *Nature* **2007**, *447*, 982−986.
(8) Casanova, O.; Iborra, S.; Corma, A. *J. Catal.* **2009**, *265*, 109−116.
(9) Demirbas, A. *Fuel Process. Technol.* **2007**, *88*, 591−597.
(10) Wiggers, V. R.; Wisniewski, A., Jr.; Madureira, L. A. S.; Chivanga Barros, A. A.; Meier, H. F. *Fuel* **2009**, *88*, 2135−2141.
(11) Garcia-Perez, M.; Shen, J.; Wang, X. S.; Li, C. Z. *Fuel Process. Technol.* **2010**, *91*, 296−305.
(12) Lédé, J.; Broust, F.; Ndiaye, F. T.; Ferrer, M. *Fuel* **2007**, *86*, 1800−1810.
(13) Asadullah, M.; Rahman, M. A.; Ali, M. M.; Rahman, M. S.; Motin, M. A.; Sultan, M. B.; Alam, M. R. *Fuel* **2007**, *86*, 2514−2520.
(14) Onay, O.; Koçkar, O. M. *Fuel* **2006**, *85*, 1921−1928.

DOI: 10.1021/acscatal.5b00303
ACS Catal. 2015, 5, 4020−4032

(15) He, R. H.; Ye, X. P.; English, B. C.; Satrio, J. A. *Bioresour. Technol.* **2009**, *100*, 5305−5311.
(16) Adam, J.; Blazsó, M.; Mészáros, E.; Stöcker, M.; Nilsen, M. H.; Bouzga, A.; Hustad, J. E.; Grønli, M.; Øye, G. *Fuel* **2005**, *84*, 1494−1502.
(17) Lohitharn, N.; Shanks, B. H. *Catal. Commun.* **2009**, *11*, 96−99.
(18) Nagaraja, B. M.; Padmasri, A. H.; Seetharamulu, P.; Hari Prasad Reddy, K.; David Raju, B.; Rama Rao, K. S. *J. Mol. Catal. A: Chem.* **2007**, *278*, 29−37.
(19) Zabaniotou, A.; Ioannidou, O.; Skoulou, V. *Fuel* **2008**, *87*, 1492−1502.
(20) Sims, R. E. H.; Mabee, W.; Saddler, J. N.; Taylor, M. *Bioresour. Technol.* **2010**, *101*, 1570−1580.
(21) Fisk, C. A.; Morgan, T.; Ji, Y. Y.; Crocker, M.; Crofcheck, C.; Lewis, S. A. *Appl. Catal., A* **2009**, *358*, 150−156.
(22) de Miguel Mercader, F.; Groeneveld, M. J.; Kersten, S. R. A.; Way, N. W. J.; Schaverien, C. J.; Hogendoorn, J. A. *Appl. Catal., B* **2010**, *96*, 57−66.
(23) Chheda, J. N.; Dumesic, J. A. *Catal. Today* **2007**, *123*, 59−70.
(24) West, R. M.; Kunkes, E. L.; Simonetti, D. A.; Dumesic, J. A. *Catal. Today* **2009**, *147*, 115−125.
(25) Huber, G. W.; Dumesic, J. A. *Catal. Today* **2006**, *111*, 119−132.
(26) Faba, L.; Díaz, E.; Ordóñez, S. *Catal. Today* **2011**, *164*, 451−456.
(27) Kaufmann, W. E.; Adams, R. *J. Am. Chem. Soc.* **1923**, *45*, 3029−3044.
(28) Sitthisa, S.; Sooknoi, T.; Ma, Y. G.; Balbuena, P. B.; Resasco, D. E. *J. Catal.* **2011**, *277*, 1−13.
(29) Rao, R. S.; Baker, R. T. K.; Vannice, M. A. *Catal. Lett.* **1999**, *60*, 51−57.
(30) Vorotnikov, V.; Mpourmpakis, G.; Vlachos, D. G. *ACS Catal.* **2012**, *2*, 2496−2504.
(31) Sitthisa, S.; Resasco, D. E. *Catal. Lett.* **2011**, *141*, 784−791.
(32) Sitthisa, S.; An, W.; Resasco, D. E. *J. Catal.* **2011**, *284*, 90−101.
(33) Sitthisa, S.; Pham, T.; Prasomsri, T.; Sooknoi, T.; Mallinson, R. G.; Resasco, D. E. *J. Catal.* **2011**, *280*, 17−27.
(34) Zheng, H. Y.; Zhu, Y. L.; Huang, L.; Zeng, Z. Y.; Wan, H. J.; Li, Y. W. *Catal. Commun.* **2008**, *9*, 342−348.
(35) Wu, J.; Shen, Y. M.; Liu, C. H.; Wang, H. B.; Geng, C. J.; Zhang, Z. X. *Catal. Commun.* **2005**, *6*, 633−637.
(36) Nagaraja, B. M.; Padmasri, A. H.; David Raju, B.; Rama Rao, K. S. *J. Mol. Catal. A: Chem.* **2007**, *265*, 90−97.
(37) Vargas-Hernández, D.; Rubio-Caballero, J. M.; Santamaría-González, J.; Moreno-Tost, R.; Mérida-Robles, J. M.; Pérez-Cruz, M. A.; Jiménez-López, A.; Hernández-Huesca, R.; Maireles-Torres, P. *J. Mol. Catal. A: Chem.* **2014**, *383*−*384*, 106−113.
(38) Xia, M. Y.; Cao, X. X.; Ni, Z. M.; Shi, W.; Fu, X. W. *Chin. J. Catal.* **2012**, *33*, 1000−1006.
(39) Greeley, J.; Mavrikakis, M. *J. Am. Chem. Soc.* **2004**, *126*, 3910−3919.
(40) Liu, B.; Greeley, J. *J. Phys. Chem. C* **2011**, *115*, 19702−19709.
(41) Mavrikakis, M.; Barteau, M. A. *J. Mol. Catal. A: Chem.* **1998**, *131*, 135−147.
(42) Tonigold, K.; Groß, A. *J. Chem. Phys.* **2010**, *132*, 224701.
(43) Jenkins, S. J. *Proc. R. Soc. London, Ser. A* **2009**, *465*, 2949−2976.
(44) Margenau, H. *Rev. Mod. Phys.* **1939**, *11*, 1−35.
(45) Bilić, A.; Reimers, J. R.; Hush, N. S. *J. Phys. Chem. B* **2002**, *106*, 6740−6747.
(46) Bilić, A.; Reimers, J. R.; Hush, N. S.; Hoft, R. C.; Ford, M. J. *J. Chem. Theory Comput.* **2006**, *2*, 1093−1105.
(47) Atodiresei, N.; Caciuc, V.; Franke, J.-H.; Blügel, S. *Phys. Rev. B: Condens. Matter Mater. Phys.* **2008**, *78*, 045411.
(48) Grimme, S. *J. Comput. Chem.* **2006**, *27*, 1787−1799.
(49) Grimme, S.; Antony, J.; Ehrlich, S.; Krieg, H. *J. Chem. Phys.* **2010**, *132*, 154104.
(50) Grimme, S.; Ehrlich, S.; Goerigk, L. *J. Comput. Chem.* **2011**, *32*, 1456−1465.
(51) Liu, B.; Cheng, L.; Curtiss, L.; Greeley, J. *Surf. Sci.* **2014**, *622*, 51−59.
(52) Wang, S. G.; Vorotnikov, V.; Vlachos, D. G. *ACS Catal.* **2015**, *5*, 104−112.
(53) Kresse, G.; Furthmüller, J. *Comput. Mater. Sci.* **1996**, *6*, 15−50.
(54) Kresse, G.; Furthmüller, J. *Phys. Rev. B: Condens. Matter Mater. Phys.* **1996**, *54*, 11169−11186.
(55) Blöchl, P. E. *Phys. Rev. B: Condens. Matter Mater. Phys.* **1994**, *50*, 17953−17979.
(56) Kresse, G.; Joubert, D. *Phys. Rev. B: Condens. Matter Mater. Phys.* **1999**, *59*, 1758−1775.
(57) Perdew, J. P.; Burke, K.; Ernzerhof, M. *Phys. Rev. Lett.* **1996**, *77*, 3865−3868.
(58) Henkelman, G.; Uberuaga, B. P.; Jónsson, H. *J. Chem. Phys.* **2000**, *113*, 9901−9904.
(59) Monkhorst, H. J.; Pack, J. D. *Phys. Rev. B* **1976**, *13*, 5188−5192.
(60) Straumanis, M. E.; Yu, L. S. *Acta Crystallogr., Sect. A: Cryst. Phys., Diffr., Theor. Gen. Crystallogr.* **1969**, *25*, 676−682.
(61) Tafreshi, S. S.; Roldan, A.; Dzade, N. Y.; de Leeuw, N. H. *Surf. Sci.* **2014**, *622*, 1−8.
(62) Johnson, O. *J. Catal.* **1973**, *28*, 503−505.
(63) Skriver, H. L.; Rosengaard, N. M. *Phys. Rev. B: Condens. Matter Mater. Phys.* **1992**, *46*, 7157−7168.
(64) Vitos, L.; Skriver, H. L.; Kollár, J. *Surf. Sci.* **1999**, *425*, 212−223.
(65) Galanakis, I.; Bihlmayer, G.; Bellini, V.; Papanikolaou, N.; Zeller, R.; Blügel, S.; Dederichs, P. H. *Europhys. Lett.* **2002**, *58*, 751−757.
(66) Da Silva, J. L.; Barreteau, C.; Schroeder, K.; Blügel, S. *Phys. Rev. B: Condens. Matter Mater. Phys.* **2006**, *73*, 125402.
(67) Wang, T.; Tian, X.-X.; Li, Y.-W.; Wang, J.; Beller, M.; Jiao, H. *ACS Catal.* **2014**, *4*, 1991−2005.
(68) Wang, T.; Wang, S.; Luo, Q.; Li, Y.-W.; Wang, J.; Beller, M.; Jiao, H. *J. Phys. Chem. C* **2014**, *118*, 4181−4188.
(69) Gao, R.; Cao, D. B.; Liu, S. L.; Yang, Y; Wang, J.; Li, Y.-W.; Jiao, H. *Appl. Catal., A* **2013**, *468*, 370−384.
(70) Little, T. S.; Qiu, J.; Durig, J. R. *Spectrochim. Acta A Mol. Biomol. Spectrosc.* **1989**, *45*, 789−794.
(71) Natal Santiago, M. A.; Sánchez-Castillo, M. A.; Cortright, R. D.; Dumesic, J. A. *J. Catal.* **2000**, *193*, 16−28.
(72) Rioux, R. M.; Vannice, M. A. *J. Catal.* **2003**, *216*, 362−376.
(73) Campbell, J. M.; Campbell, C. T. *Surf. Sci.* **1991**, *259*, 1−17.
(74) Rettner, C. T.; Michelsen, H. A.; Auerbach, D. J. *Faraday Discuss.* **1993**, *96*, 17−31.
(75) Kratzer, P.; Hammer, B.; Nørskov, J. K. *Surf. Sci.* **1996**, *359*, 45−53.
(76) Tang, Q. L.; Chen, Z. X.; He, X. A. *Surf. Sci.* **2009**, *603*, 2138−2144.
(77) Gokhale, A. A.; Dumesic, J. A.; Mavrikakis, M. *J. Am. Chem. Soc.* **2008**, *130*, 1402−1414.
(78) Phatak, A. A.; Delgass, W. N.; Ribeiro, F. H.; Schneider, W. F. *J. Phys. Chem. C* **2009**, *113*, 7269−7276.
(79) Shustorovich, E. *Adv. Catal.* **1990**, *37*, 101−163.
(80) Pang, X. Y.; Xue, L. Q.; Wang, G. C. *Langmuir* **2007**, *23*, 4910−4917.
(81) Wang, G. C.; Tao, S. X.; Bu, X. H. *J. Catal.* **2006**, *244*, 10−16.
(82) Tang, Q. L.; Chen, Z. X. *Surf. Sci.* **2007**, *601*, 954−964.
(83) Zhang, P.; Zheng, W. T.; Jiang, Q. *J. Phys. Chem. C* **2010**, *114*, 19331−19337.
(84) Kandoi, S.; Gokhale, A. A.; Grabow, L. C.; Dumesic, J. A.; Mavrikakis, M. *Catal. Lett.* **2004**, *93*, 93−100.
(85) Au, C.-T.; Breza, J.; Roberts, M. W. *Chem. Phys. Lett.* **1979**, *66*, 340−343.
(86) Liu, S. L.; Tian, X. X.; Wang, T.; Wen, X. D.; Li, Y.-W.; Wang, J.; Jiao, H. *J. Phys. Chem. C* **2014**, *118*, 26139−26154.
(87) Liu, S. L.; Tian, X. X.; Wang, T.; Wen, X. D.; Li, Y.-W.; Wang, J.; Jiao, H. *Phys. Chem. Chem. Phys.* **2015**, *17*, 8811−8821.
(88) Pang, S. H.; Medlin, J. W. *ACS Catal.* **2011**, *1*, 1272−1283.

DOI: 10.1021/acscatal.5b00303
ACS Catal. 2015, 5, 4020−4032